



1 **Carbon geochemistry of plankton-dominated supra-micron samples in the Laptev and**

2 **East Siberian shelves: contrasts in suspended particle composition**

3 Tesi Tommaso^{1,2,3}, Marc C. Geibel^{1,2}, Cristoph Pearce^{4,5}, Elena Panova⁶, Jorien E. Vonk⁷,

4 Emma Karlsson^{1,2}, Joan A. Salvado^{1,2}, Martin Kruså^{1,2}, Lisa Bröder^{1,2}, Christophe Humborg

5 ^{1,2}, Igor Semiletov^{6,8,9}, Örjan Gustafsson^{1,2}

6

7 ¹ Department of Environmental Science and Analytical Chemistry (ACES), Stockholm

8 University

9 ² Bolin Centre for Climate Research, Stockholm University

10 ³ Institute of Marine Sciences, National Research Council (ISMAR-CNR)

11 ⁴ Department of Geological Sciences, Stockholm University, Sweden

12 ⁵ Department of Geoscience, Aarhus University, Denmark

13 ⁶ Tomsk Polytechnic University

14 ⁷ Vrije Universiteit Amsterdam (VU)

15 ⁸ Pacific Oceanological Institute FEB RAS

16 ⁹ University of Alaska Fairbanks

17

18

19

20

21

22

23

24

25



26

27 **Abstract**

28 Recent Arctic studies suggest that sea-ice decline and permafrost thawing will affect
29 phytoplankton dynamics and stimulate marine heterotrophic communities. However, in what
30 way the plankton composition will change as the warming proceeds remains elusive. Here we
31 investigate the chemical signature and plankton speciation of the supra-micron ($> 10 \mu\text{m}$)
32 particulate organic matter (supra-POM) fraction collected along the Siberian shelf. Supra-
33 POM samples were analysed at bulk ($\delta^{13}\text{C}$ and $\Delta^{14}\text{C}$) and molecular level (CuO oxidation and
34 IP_{25}) while plankton identification established the dominant taxa. In addition, surface water
35 chemical properties were integrated with the plankton dataset to understand the link between
36 plankton composition and environmental conditions.

37 The dual-carbon isotope fingerprint indicates a large variability in the supra-POM
38 distribution while terrestrial biomarkers suggest negligible land-derived input. In the open-
39 waters of the outer Laptev Sea (LS), heterotrophic plankton dominated the assemblages. $\delta^{13}\text{C}$
40 and $\Delta^{14}\text{C}$ suggest that modern terrestrial dissolved organic carbon (DOC) from the Lena river
41 is the primary source of metabolizable carbon which is transferred to the heterotrophic
42 communities via microbial loops. Moving eastwards toward the sea-ice dominated East
43 Siberian Sea (ESS), the system became progressively more autotrophic and dominated by sea-
44 ice and pelagic diatoms which is confirmed. Comparison between $\delta^{13}\text{C}$ of supra-POM
45 samples and CO_2aq concentrations suggests that the carbon isotope fractionation follows the
46 general growth vs CO_2aq supply model with the highest $\delta^{13}\text{C}$ values found in the easternmost,
47 most productive stations.

48 In a warming scenario characterized by enhanced terrestrial release and further sea-ice
49 decline, heterotrophic conditions fuelled by terrestrial DOC will likely persist in the LS while



50 ESS might experience enhanced primary productivity. This will result in a sharp
51 compositional gradient similar to what documented in our semi-synoptic study.

52

53 **1. Introduction**

54 The progressive reduction of sea-ice extent in the Arctic Ocean is indisputable
55 evidence of modern global warming (Comiso et al., 2008; Kwok and Rothrock, 2009). The
56 unprecedented decline of sea-ice is expected to alter several aspects of the Arctic marine
57 ecology such as plankton abundance and its temporal distribution (Arrigo et al., 2008). For
58 instance, recent studies suggest that the increase of solar irradiance will stimulate greater
59 primary productivity in summer while the prolonged ice-free conditions will develop a second
60 algal bloom in early fall, which is a distinctive feature of only lower latitudes (Ardyna et al.,
61 2014; Lalande et al., 2009; Lalande et al., 2014). The phytoplankton communities are
62 expected to profoundly change towards a higher contribution from open water phytoplankton
63 at the expense of sea-ice assemblages (Fujiwara et al., 2014). Taken together, a greater
64 productivity in the ice-free or marginal ice zone compare to in the inner multi-year ice system,
65 is also expected to lead to greater uptake and settling export of organic carbon from the
66 surface to deeper strata of the Arctic Ocean (Gustafsson and Andersson, 2012).

67 Sea-ice decline will also project to water-air gas exchange, currents and river plume
68 dispersion which, in turn, exert large control on the surface water chemical/physical
69 properties (Aagaard and Carmack, 1989; Ardyna et al., 2014; Lalande et al., 2014). On top of
70 this, destabilization of several aspects of permafrost and hydrology on land will results in
71 enhanced particulate and dissolved carbon input to the Arctic Ocean (Frey and Smith, 2005;
72 Vonk et al., 2012). Thus, the geochemical signature of both autotrophic and heterotrophic
73 plankton communities is also expected to change as the warming proceeds. However, how the
74 cryosphere destabilization will ultimately affect the marine geochemical signal is poorly



75 understood. This study seeks a better understanding of the chemical composition of plankton
76 that dominates regions of the Arctic Ocean characterized by different sea-ice coverages and
77 terrestrial input. In particular, we focus on the carbon isotope fingerprint (i.e., $\delta^{13}\text{C}$ and $\Delta^{14}\text{C}$)
78 of plankton that grows in ice-covered and ice-free Marginal Ice Zone (MIZ) regimes in the
79 river-dominated Siberian margin. The motivation behind investigating the chemical
80 fingerprint of plankton from different sea-ice domains is to provide a better understanding of
81 the carbon signature for direct applications to carbon studies of both modern systems and
82 paleo-reconstructions. In particular, the isotope composition of marine OC finds several
83 applications in climate, ecology and carbon source apportionment studies. For example, stable
84 carbon isotopes of marine phytoplankton are used for paleo- $p\text{CO}_2$ reconstructions over
85 geological time scales (Hoins et al., 2015; Pagani et al., 1999; Popp et al., 1999; Rau, 1994).
86 The $\delta^{13}\text{C}$ signature also provides a solid tool for marine food web and ecosystem structure
87 investigations (Dunton et al., 2006; Iken et al., 2005; Kohlbach et al., 2016). Furthermore,
88 dual-carbon isotope mixing models ($\delta^{13}\text{C}$ and $\Delta^{14}\text{C}$) are commonly used to quantify the
89 relative proportion of marine and various allocthonous sources (e.g., permafrost soil) in both
90 contemporary and paleo-reconstructed carbon cycling of the Arctic (Karlsson et al., 2016;
91 Tesi et al., 2016; Vonk et al., 2012; Vonk et al., 2014).

92 With this overarching goal in mind, here we investigate the $>10\ \mu\text{m}$ (supra-micron)
93 fraction of particulate organic matter (supra-POM) in ice-covered and ice-free MIZ regimes
94 of the Siberian Arctic Shelf during the SWERUS-C3 expedition (July-August 2014) (Fig. 1).
95 The plankton-dominated supraPOC samples collected throughout the ca. 4,500 km long cruise
96 track were characterized at bulk (OC, $\delta^{13}\text{C}$ and $\Delta^{14}\text{C}$) and biomarker level (highly branched
97 isoprenoids, IP₂₅; CuO oxidation products) while plankton identification via microscope
98 provided information about the dominant assemblages. In addition, continuous measurements
99 of dissolved CO_2 ($\text{CO}_{2\text{aq}}$) and its stable carbon isotope composition ($\delta^{13}\text{C}_{\text{CO}_2}$) were performed



100 during the campaign for a direct comparison with the chemical composition of the supra-POM
101 fraction.

102

103 2. Methods

104 2.1 Supra-micron fraction sampling

105 Seawater was pumped from a stainless steel inlet on the hull of the icebreaker *Oden*
106 positioned at 8 m below the sea surface. The inlet system is tested and further described in
107 Sobek and Gustafsson (2004) and Gustafsson et al. (2005). Figure 1a shows the region
108 covered to harvest each supra-POM samples. The particulate material was retained via a large
109 volume filtration apparatus using a 10- μm Nitex® (nylon) mesh placed in a 29.3 cm filter
110 holder. After collection, filtered samples were rinsed with MilliQ water and the particulate
111 material (i.e., supra-micron fraction) was kept frozen throughout the expedition. In the lab,
112 samples were transferred in pre-cleaned Falcon® tubes and centrifuged to remove the
113 supernatant. The residual particulate material was frozen and subsequently freeze-dried prior
114 to biogeochemical analyses.

115 In all figures, sample location of the supra-POM samples refers to its time-averaged
116 position as shown in Figure 1.

117

118 2.2 Bulk carbon isotopes and biomarker analyses

119 Organic carbon (OC) and stable carbon isotope ($\delta^{13}\text{C}$) analyses were carried out on
120 acidified samples (Ag capsules, HCl, 1.5M) to remove the carbonate fraction (Nieuwenhuize
121 et al., 1994). Analyses were performed using a Thermo Electron mass spectrometer directly
122 coupled to a Carlo Erba NC2500 Elemental Analyzer via a Conflo III (Department of
123 Geological Sciences, Stockholm University). OC values are reported as weight percent
124 (%d.w.) whereas stable isotope data are reported in the conventional $\delta^{13}\text{C}$ notation (‰). The



125 analytical error for $\delta^{13}\text{C}$ was lower than $\pm 0.1\%$ based on replicates. Acidified (HCl, 1.5 M)
126 samples for radiocarbon abundance were analysed at the US-NSF National Ocean Science
127 Accelerator Mass Spectrometry (NOSAMS) facility (Woods Hole Oceanographic Institution,
128 Woods Hole, USA). Radiocarbon data are reported in the standard $\Delta^{14}\text{C}$ notation (‰).

129 Alkaline CuO oxidations were carried out using an UltraWAVE Milestone microwave
130 as described in Tesi et al. (2014). Briefly, about 2 mg of OC was oxidised using CuO under
131 alkaline (2N NaOH) and oxygen-free conditions at 150 °C for 90 min in teflon tubes. After
132 the oxidation, known amounts of recovery standards (trans-cinnamic acid and ethylvanillin)
133 were added to the solution. The NaOH solutions were then acidified to pH 1 with
134 concentrated HCl and extracted with ethyl acetate. Extracts were dried and redissolved in
135 pyridine. CuO oxidation products were quantified by GC-MS in full scan mode (50-650 m/z).
136 Before GC analyses, the CuO oxidation products were derivatized with bis(trimethylsilyl)
137 trifluoroacetamide+1% trimethylchlorosilane at 60°C for 30 min. The compounds were
138 separated chromatographically in a 30m×250 μm DB5ms (0.25 μm thick film) capillary GC
139 column, using an initial temperature of 100°C, a temperature ramp of 4°C/min and a final
140 temperature of 300°C. Lignin phenols (terrestrial biomarkers) were quantified using the
141 response factors of commercially available standards (Sigma-Aldrich) whereas the rest of the
142 CuO oxidation products were quantified by comparing the response factor of trans-cinnamic
143 acid. Lignin-derived reaction products include vanillyl phenols (V=vanillin, acetovanillone,
144 vanillic acid), syringyl phenols (S=syringaldehyde, acetosyringone, syringic acid) and
145 cinnamyl phenols (C=p-coumaric acid, ferulic acid). In addition to lignin, cutin-derived
146 products (hydroxyl fatty acids) were used to trace the land-derived input (Goñi and Hedges,
147 1990; Tesi et al., 2010). Other CuO oxidation products include para-hydroxybenzene
148 monomers (P-series), benzoic acids (B-series) and short-chain fatty acids (FA-series) which
149 can have both terrestrial and marine origin (Goñi and Hedges, 1995; Tesi et al., 2010).



150 IP₂₅ (monounsaturated highly branched isoprenoid) was quantified according to Belt et
151 al. (2012). Briefly, lipids were extracted via sonication using a dichloromethane/methanol
152 solution (2:1 v/v × 3). Prior to the extraction, two internal standards (7-hexylnonadecane, 7-
153 HND and 9-octylheptadecene, 9-OHD) were added to permit quantification of IP₂₅
154 (monounsaturated highly branched isoprenoid) following analysis via GC-MS. Total lipid
155 extracts (TLEs) were dried under N₂ after removing the water excess with anhydrous NaSO₄.
156 Dry TLEs were redissolved in dichloromethane and the non-polar hydrocarbon fraction was
157 purified using open column chromatography (activated SiO₂) and hexane as eluent. Saturated
158 and unsaturated n-alkanes were further separated using 10% AgNO₃ coated silica gel using
159 hexane and dichloromethane, respectively.

160 Quantification of IP₂₅ was carried out in SIM mode (*m/z* 350.3) as described in Belt et
161 al. (2012). The GC was fitted with a 30m×250 μm DB5ms (0.25 μm thick film) capillary GC
162 column. Initial GC oven temperature was set to 60°C followed by a 10°C/min ramp until a
163 final temperature of 310°C (hold time 10 min).

164

165 **2.3. Microscope images of plankton**

166 High resolution digital images were taken with an Environmental Scanning Electron
167 Microscope (ESEM) Philips XL30 FEG in high voltage (15kV) and magnification 250X.
168 Samples were further studied for identification of diatoms and dinoflagellates using a
169 transmitted light microscope (Leitz Laborlux 12 Pol) equipped with differential interference
170 contrast optics at 1000X magnification.

171

172 **2.4 WEGAS measurements of CO₂aq**

173 Cavity ring-down spectrometer (CRDS) measurements were used to continuously
174 monitor CO₂ concentrations and δ¹³C_{CO2} composition of gas stripped via headspace



175 equilibration from the water column using the Water Equilibration Gas Analyser System
176 (WEGAS) (Thornton et al. 2016). It consists of three major components:
177 a) Water handling system including i) showerhead equilibrator (head space volume 1 L) fed
178 by the sea water intake described above, ii) continuous pH measurements by E&H electrode
179 probe and iii) T and salinity measurements by Seabird TSG 45.
180 b) CRDS gas analyzers for CO₂ stable carbon isotopes (model G2131-i, Picarro Inc.,
181 Sunnyvale, CA) and CO₂ concentrations (model G2301, Picarro Inc., Sunnyvale, CA).
182 c) Gas handling system with circulation pumps for headspace and ambient air from
183 meteorological tower.

184 Continuous measurements of surface water CO₂ and δ¹³C_{CO₂}, were thus performed
185 using IB/Oden's seawater intake. Water was pumped through spray nozzles into the open
186 headspace equilibrator at ~4.5 L min⁻¹. By creating a fine spray of droplets, the exchange
187 surface between headspace and water is maximized and an optimal equilibration is achieved.
188 The gas of the headspace was analysed using two different CRDS (cavity ring-down)
189 analysers. The second analyser was operated in parallel and its flow (~25 mL min⁻¹) was not
190 fed back into the closed cycle. Thus, it created a defined vent flow. This vent flow is
191 compensated by a flow of ambient air (AA) taken from the top inlet of the meteorological
192 tower (20 m height). To be able to correct the data for the vent flow, the concentration of CO₂
193 and δ¹³C_{CO₂} in AA is monitored by frequent switching. During the SWERUS-C3 expedition,
194 continuous CO₂ and δ¹³C-CO₂ measurements in the surface waters have been performed in
195 the period 10 July - 9 August resulting in a total of 238 864 data points.

196 For this study all measurement data taken within a time window of +/-5min around the
197 specific start times of the sample taking were averaged to account for filling time of the
198 canister and residence time of the water in the SWI.



199

200 **2.5 Sea-ice data**

201 Daily AMSR2 sea-ice extent and concentration maps were provided by the Institute of
202 Environmental Physics, University of Bremen, Germany (Spren et al., 2008) as GeoTIFF
203 files (<ftp://seaice.uni-bremen.de>).

204

205 **3. Results and discussion**

206 **3.1 Surface water conditions**

207 Before discussing the chemical composition of the supra-POM fraction, here we
208 briefly introduce the different environmental conditions encountered throughout the cruise
209 track. The surface water data presented in this section were pulled together from previous
210 studies which provide an in-depth analysis of the surface water properties during the
211 SWERUS-C3 expedition (Humborg et al., submitted; Salvadó et al., 2016; The SWERUS-C3
212 Scientific Party, 2016) (Table 2). For this study, continuous CO₂aq and $\delta^{13}\text{C}_{\text{CO}_2}$ data
213 (Humborg et al., submitted; The SWERUS-C3 Scientific Party, 2016) acquired throughout the
214 expedition were organized to match the water sampling stations allowing for a direct
215 comparison with DOC and salinity data (Fig. 2).

216 Summer 2014 was consistent with the long-term downward trend in Arctic sea-ice
217 extent. The strongest anomalies were observed in the LS which experienced the most
218 northerly sea-ice shift since satellite observations began in 1979. In general, sea-ice displayed
219 a strong gradient over the study region going from ice-free conditions in the outer LS to ice-
220 dominated waters in the outer ESS. Figure 1 displays sea-ice extent and concentration at the
221 beginning, in the middle and at the end of the sampling. Furthermore, Table 1 reports the
222 averaged sea-ice concentrations for each sample.



223 The surface water salinity exhibited a longitudinal trend characterized by low values
224 in the outer LS while the sea-ice dominated ESS waters showed relatively higher values (Fig.
225 2a; Table 2). However, the highest salinity values were measured in the westernmost stations
226 resulting in a sharp gradient in the LS. The low surface water salinities in the outer LS are
227 most likely the result of both Lena river input and sea-ice thawing (Humborg et al., submitted;
228 The SWERUS-C3 Scientific Party, 2016) that started in late May (Janout et al., 2016).

229 The highest DOC concentrations were measured in the mid-outer LS in the surface
230 water plume affected by Lena River runoff (Fig.2b; Table 2). Overall, DOC concentrations
231 mirrored the salinity distribution with high DOC concentrations corresponding to low
232 salinities (Fig. 2). Carbon stable isotopes ($\delta^{13}\text{C}$) and terrestrial biomarkers (of the solid-phase
233 extracted DOC fraction; Salvado et al., 2016) further confirmed the influence of terrestrial
234 DOC in the outer LS, while the terrestrial imprint decreased moving eastward.

235 CO_2aq concentrations exhibited a typical estuarine pattern over the study region
236 (Humborg et al., submitted; The SWERUS-C3 Scientific Party, 2016) (Fig. 2d; Table 2). Low
237 salinity waters in the outer LS showed above atmospheric CO_2 concentrations (i.e.,
238 oversaturation) while surface waters below sea-ice exhibited undersaturated concentrations.
239 The most depleted $\delta^{13}\text{C}_{\text{CO}_2}$ values were measured off the Lena river mouth (Humborg et al.,
240 submitted; The SWERUS-C3 Scientific Party, 2016) (Fig. 2e; Table 2). Being relatively rich
241 in land-derived material, it is likely that respired terrestrial OC within the river plume exerted
242 control on the CO_2 isotopic signature and concentration.

243 Finally, nutrient distribution revealed nitrate (NO_3) and nitrite (NO_2) depletion in
244 surface waters throughout the cruise track (Humborg et al., submitted; The SWERUS-C3
245 Scientific Party, 2016). Phosphate (PO_4) exhibited rather low concentrations in the outer LS
246 and relatively higher concentrations below the sea-ice in the outer ESS (Humborg et al.,



247 submitted; The SWERUS-C3 Scientific Party, 2016) likely reflecting the Pacific inflow
248 (Semiletov et al., 2005).

249

250 **3.2 Source of the supra-micron POM fraction**

251 The Arctic Ocean off northern Siberia receives large quantities of dissolved and
252 particulate terrestrial organic carbon (TerrOC) via continental runoff and coastal erosion
253 (Alling et al., 2010; Dittmar and Kattner, 2003; McClelland et al., 2016; Sánchez-García et
254 al., 2011; Semiletov et al., 2013; Vonk et al., 2012). The land-derived material that does not
255 settle in the coastal zone further travels across the margin reaching out to the outer-shelf
256 region resuspended within the benthic nepheloid layer or in suspension within the surface
257 river plume (Fichot et al., 2013; Sánchez-García et al., 2011; Wegner et al., 2003). Thus, we
258 addressed to what extent TerrOC affects the supra-POM fraction by quantifying the
259 concentration of lignin phenols and C16-18 hydroxy fatty acids (cutin-derived products).
260 These biomarkers are exclusively formed by terrestrial vegetation and, thus, serve as tracers
261 of TerrOC in the marine Arctic environment (Amon et al., 2012; Bröder et al., 2016b; Feng et
262 al., 2015).

263 Upon CuO alkaline oxidation the supra-POM samples yielded only traces of lignin
264 phenols while the cutin-derived products were not detected (Fig. 3). Other oxidation products
265 in high abundance included saturated and mono-unsaturated short chain fatty acids (C12-
266 18FA), para-hydroxy phenols, benzoic acids and dicarboxylic acids. These other reaction
267 products are ubiquitous in both marine and terrestrial environments but they are predominant
268 in plankton-derived material, especially short-chain fatty acids. When compared with active-
269 layer permafrost soils and ice-complex deposits (Tesi et al., 2014), supra-POM samples
270 displayed a distinct CuO fingerprint dominated by short chain fatty acids (Fig. 3), consistent
271 with the typical CuO fingerprints of phytoplankton batch cultures (Goñi and Hedges, 1995).



272 SEM images further corroborated the abundance of marine plankton detritus in the supra-
273 POM fraction while lithogenic particles (clastic material) appeared to be sporadic in all
274 samples.

275 The OC content (% d.w.) of the supra-POM fraction decreased eastwards showing
276 high concentrations in the LS and relatively low values in the ESS (Table 1). However, in
277 terms of absolute concentration in the water column ($\mu\text{C/l}$), the highest levels were generally
278 observed in the sea-ice covered region (Table 1; Fig. 4a). Qualitative analyses by SEM and
279 transmitted-light microscopy highlight important differences in plankton assemblages which
280 reflect different timing of the plankton blooms which can explain these differences in
281 concentration. Specifically, the open-water LS stations exhibited a low degree of plankton
282 diversity and were largely dominated by a bloom of heterotrophic dinoflagellate cysts
283 (*Protoperidinium* spp) (Fig. 5a; Table 3). Moving towards the ice-dominated regions, diatoms
284 become the prevailing species. Dominant diatom genera include *Chaetoceros* spp. (dominant
285 diatom in several stations), *Thalassiosira* spp., *Rhizosolenia* spp., *Coscinodiscus* spp.,
286 *Asteromphalus* spp., *Navicula* spp. as well as sea-ice species such as *Fragilariopsis cylindrus*
287 and *Fragilariopsis oceanica* (Fig. 5b,c; Table 3).

288 A moored line deployed in the LS shelf recorded the sea-ice retreat in 2014 and found
289 no sign of pelagic under-ice blooms despite available nutrients while high chlorophyll
290 concentrations were detected immediately after the ice retreated in late May (Janout et al.,
291 2016). The ice-edge blooms lasted for about 2 weeks according to the high resolution
292 chlorophyll time-series (Janout et al., 2016). Thus, our post-bloom sampling in the LS
293 essentially captured an oligotrophic environment (Gustafsson et al., 2016) dominated by
294 heterotrophic dinoflagellate cysts (i.e. *Protoperidinium* spp) which likely fed on phytodetritus
295 and river-derived organic material. Such conditions are fairly consistent with the relatively
296 low carbon contents observed in LS waters (Fig. 4a).



297 The Arctic sea-ice biomarker IP25 (Fig. 4b) further corroborated the sampling of
298 different plankton taxa in ice-free and ice-dominated surface waters. IP25 is a proxy of sea-ice
299 based on a highly branched mono-unsaturated isoprenoid alkene found in some sea-ice
300 diatoms which, however, generally account for 5% of the total sea-ice taxa (Belt et al., 2007;
301 Brown et al., 2014). The IP25 concentrations varied by several orders of magnitude over the
302 study area showing low concentrations in the open-water western region while the sea-ice
303 dominated surface waters to the east exhibited high concentrations especially at station 31b
304 (Fig. 4b; Table 1). The fact that IP25 was still detectable throughout the ice-free outer LS
305 suggests that the proxy captured the signal of the sea-ice retreat that occurred shortly before
306 the sampling at the end of May/early June (Janout et al., 2016).

307

308 3.3. $\delta^{13}\text{C}$ and $\Delta^{14}\text{C}$ of the supra-micron POM fraction

309 $\delta^{13}\text{C}$ and $\Delta^{14}\text{C}$ of the supra-POM fraction also exhibited a distinctive longitudinal
310 trend across the study area (Fig. 4c,d).

311 Depleted $\delta^{13}\text{C}$ values characterized the LS open waters ranging from -28.1 to -24.7‰
312 (Fig. 4c). Although within the range of terrestrially-derived material, our CuO oxidation data
313 (i.e. trace of lignin phenols and absence of cutin-derived products) suggest that the “light”
314 isotopic composition in the LS might instead reflect the plankton assemblage dominated by
315 heterotrophic dinoflagellate cysts as previously described (e.g., *Protoperidinium* spp; Fig. 5a).
316 More specifically, heterotrophic dinoflagellates can adapt their metabolism depending on the
317 substrate available (e.g., diatoms and bacteria). Several studies have shown that terrestrial
318 DOC greatly promotes bacteria biomass production which in turn stimulates the growth of
319 heterotrophic dinoflagellates (Carlsson et al., 1995; Purina et al., 2004; Wikner and
320 Andersson, 2012). Thus, in these conditions, allochthonous terrestrial DOC is actively



321 recycled by bacteria and transferred to dinoflagellates which explains, thus, the depleted $\delta^{13}\text{C}$
322 values observed in the river-dominated samples (Carlsson et al., 1995).

323 The modern radiocarbon fingerprint of the Lena DOC discharge is consistent with
324 $\Delta^{14}\text{C}$ signature of the supra-POM fraction in the LS (up to +99 ‰), supporting, thus, the DOC
325 microbial loop within the river plume (Fig. 4d and 6). By contrast, comparison with other
326 potential carbon sources which include the Lena river particulate organic carbon, surface
327 sediments, Pleistocene coastal Ice-Complex Deposit and Pacific DIC inflow reveals a
328 different (more depleted) radiocarbon fingerprint (Fig. 6).

329 Moving towards the ice-dominated ESS, surface waters progressively become more
330 autotrophic and productive (Humborg et al., submitted; The SWERUS-C3 Scientific Party,
331 2016) while the supra-POM exhibited a wide $\delta^{13}\text{C}$ signature ranging from -28.6 to -21.2‰
332 (Fig. 4c). The most depleted values were observed across the transition zone between open-
333 waters and sea-ice. Visual inspections of these samples revealed large abundance of the
334 centric diatom *Chaetoceros* spp. (spores and vegetative cells; St22, Fig. 5b) while lignin and
335 cutin data indicated, a negligible input of land-derived material. Primary factors determining
336 the fractionation of stable carbon isotopes in phytoplankton are several and include CO_2aq
337 concentration, $\delta^{13}\text{C}_{\text{aq}}$, growth rate, cell size, cell shape, light and nutrient availability
338 (Gervais and Riebesell, 2001; Laws et al., 1997a; Popp et al., 1998; Rau et al., 1996). Our
339 understanding about isotopic fractionation has been historically achieved via laboratory
340 experiments designed to test each factor under controlled conditions. In natural environments,
341 however, different factors can compete with each other, sometimes in opposite directions.
342 Yet, the existing knowledge about surface water properties during the expedition (Humborg et
343 al., submitted; The SWERUS-C3 Scientific Party, 2016) can provide important constraints for
344 the isotopic signal interpretation.



345 For example, comparison with continuous $\delta^{13}\text{C-CO}_2\text{aq}$ and CO_2aq data measured
346 throughout the cruise track - time-averaged to match the large volume filtration along the
347 cruise track (Table 1) - suggested a negligible role exerted by $\delta^{13}\text{C-CO}_2\text{aq}$ (Fig. 7b) while
348 CO_2aq concentration correlated with the $\delta^{13}\text{C}$ of the supra-POM fraction ($r^2=0.72$) (Fig. 7a).
349 Such a relationship fits with the general model according to which a low demand (i.e., low
350 growth rate) and high supply (i.e., abundant CO_2aq) favour high fractionation and vice versa
351 (Laws et al., 1997b; Laws et al., 1995; Wolf-Gladrow et al., 1999).

352 During the expedition, surface water properties (i.e. O_2 and CO_2 , Table 2) (Humborg
353 et al., submitted; The SWERUS-C3 Scientific Party, 2016) suggest that the productivity in the
354 outer ESS increases moving eastward, as commonly observed, likely due to the Pacific inflow
355 (Björk et al., 2011; Semiletov et al., 2005). Thus, the wide range of plankton $\delta^{13}\text{C}$ over the
356 ESS can be explained in terms of two different regimes: (a) in the transition zone between
357 open waters and sea-ice, the productivity was low but CO_2aq was oversaturated while (b) in
358 the easternmost ESS, productivity was high but CO_2aq was depleted (Fig. 7b). The former
359 regime favours fractionation while the latter does not (Fig. 7b). Different diatom assemblages
360 can also be another factor to consider although the phytoplankton diversity observed over ESS
361 can be considered rather small (e.g. *Chaetoceros spp.* dominant in most of the samples)
362 compared to the wide range of $\delta^{13}\text{C}$ observed (i.e., from -28.8 to -21.6) (Table 3).

363 The supra-POM fraction in the sea-ice dominated ESS exhibited slightly - but
364 consistently - depleted $\Delta^{14}\text{C}$ values ranging from -62 to -49 ‰ (Fig. 4d). This region is
365 affected by the inflow of Pacific waters whose DIC exhibits, however, a modern $\Delta^{14}\text{C}$
366 signature (Griffith et al., 2012) (Fig. 6). By contrast, these results suggest the influence from
367 an aged carbon pool. As the ESS remains covered by sea-ice for most of the year, it is
368 possible that the sea-ice hampers the gas exchange with the atmosphere and acts as a lid by
369 trapping CO_2 which derives from the breakdown of sedimentary organic material (Anderson



370 et al., 2009; Semiletov et al., 2016), which might have such ages (Bröder et al., 2016a; Vonk
371 et al., 2012). In these conditions, the pre-aged CO₂ accumulates underneath the sea-ice and is
372 subsequently incorporated during carbon fixation by the phytoplankton. While oversaturated
373 bottom waters were extensively documented in the region with important consequences on the
374 local DIC (Anderson et al., 2009; Pipko et al., 2009), more work is clearly needed to
375 understand if early diagenesis in sediments can also affect the radiocarbon signature of the
376 CO₂aq underneath the sea-ice. Alternatively, the slightly depleted radiocarbon signature might
377 indicate the presence of pre-aged terrestrial organic carbon (Fig. 6) in the supra-POM
378 samples, not reflected in the lignin and cutin tracers (Fig. 3). However, it would then remain
379 elusive why such an aged land-derived influence was not visible in the river-dominated LS
380 waters while it affected the sea-ice dominated region.

381 Taken together, our results indicate that the dual-carbon isotope fingerprint is highly
382 affected by the trophic conditions (heterotrophic *vs* autotrophic) as well as the extent of
383 primary productivity. In a warming scenario characterized by sea-ice retreat (Arrigo et al.,
384 2008; Comiso et al., 2008) and enhanced terrestrial input from land as result of hydrology and
385 permafrost destabilization (Frey and Smith, 2005; Vonk et al., 2012), the geochemical
386 composition of plankton will likely change as the warming proceeds.

387

388 **Conclusions**

389 Analyses of large-volume filtrations of plankton-dominated >10 µm particle samples
390 revealed a high degree of heterogeneity in geochemical and plankton composition with an in
391 between ice-free. Thus, the dual-carbon isotope fingerprint of the plankton-dominated fraction
392 reflects a contemporary terrestrial DOC signature (i.e., depleted δ¹³C and modern Δ¹⁴C
393 fingerprint). Heterotrophic dinoflagellates dominated the plankton assemblages in this ice-free
394 region. Hence, results suggest a heterotrophic environment in the outer LS open waters where



395 the river-derived DOC is transferred to relatively higher trophic levels via microbial
396 incorporation (i.e, microbial loop).

397 Moving eastwards towards the ice-dominated outer ESS, surface waters became
398 progressively more autotrophic and largely dominated by diatoms. Here, the isotopic
399 fractionation appears to follow the growth vs CO₂ demand model according to which carbon
400 fractionation increases at low growth and high CO₂ supply. As a result, the transition between
401 open-waters and sea-ice exhibited more depleted δ¹³C values compared to the productive
402 easternmost stations. Radiocarbon signatures were slightly depleted over the whole sea-ice
403 dominated area. This raises the question whether the sea-ice hampers the gas exchange with
404 the atmosphere and trap the CO₂ sourced from reactive sedimentary carbon pools.

405 In a warming scenario, it is likely that the oligotrophic ice-free LS will be dominated
406 by heterotrophic metabolism fuelled by terrestrially-derived organic material (i.e., Lena
407 input). In these conditions, the dual-carbon isotope signature of the heterotrophic plankton
408 will essentially reflect the terrestrial input. In the ESS, which receives the inflow of the
409 nutrient-rich Pacific waters, ice-free conditions will promote the light penetration. This in turn
410 might further stimulate phytoplankton growth with important implications in terms of CO₂
411 depletion and resulting low isotope fractionation. It is likely that this will result in a sharp
412 compositional gradient (e.g. δ¹³C) between LS and ESS similar to what has already been
413 captured in our semi-synoptic study.

414

415 **Acknowledgements**

416 We thank the *I/B Oden* crew and the Swedish Polar Research Secretariat staff. This
417 study was supported by the Knut and Alice Wallenberg Foundation (KAW contract
418 2011.0027), the Swedish Research Council (VR contract 621-2007-4631 and 621-2013-
419 5297), European Research Council (ERC-AdG CC-TOP project #695331 to Ö.G.). T. Tesi



420 additionally acknowledges EU financial support as Marie Curie fellow (contract no. PIEF-
421 GA-2011-300259). J.A. Salvadó acknowledges EU financial support as a Marie Curie grant
422 (contract no. FP7-PEOPLE-2012-IEF; project 328049). I. Semiletov acknowledges financial
423 support from the Russian Government (grant No. 14, Z50.31.0012/03.19.2014) and the
424 Russian Foundation for Basic Research (nos. 13-05-12028 and 13-05-12041), and E. Panova
425 from the Russian Scientific Foundation (grant no. 15-17-20032). We thank the Arctic Great
426 Rivers Observatory (NSF-1107774) for providing DOC and POC river data
427 (www.arcticgreatrivers.org).

428

429

430

431

432

433

434

435

436

437

438

439

440

441

442

443

444



445

446

447

448

449

Table 1. Supra-micron POM (supraPOM) composition and continuous CO₂aq measurements

ID	Time averaged latitude (N)	Time averaged longitude (E)	Mean sea-ice percentage (%)	Supra-micron POM concentration (mg/l)	OC (d.w.)	TN (d.w.)	$\delta^{13}\text{C}$ (‰)	$\Delta^{14}\text{C}$ (‰)	IP25 (ng/gOC)	average CO ₂ aq (ppm)	average $\delta^{13}\text{C}$ -CO ₂ aq (‰)
ST4	81.68	105.96	98.4	6	18.2	3.3	-26.7	n.d.	n.d.	323	-10.9
ST5	80.47	114.07	98.7	15	42.6	3.5	-27.6	n.d.	n.d.	322	-11.0
ST6	78.86	125.22	82.2	1	51.7	3.3	-26.6	99	n.d.	325	-10.8
ST7	77.88	126.62	0.0	11	43.1	2.5	-25.7	n.d.	88	350	-10.7
ST8	77.16	127.32	0.0	17	30.9	2.9	-26.7	41	n.d.	391	-10.5
ST9	76.78	125.83	0.0	3	31.5	3.7	-27.9	30	48	385	-10.5
ST10	76.90	127.81	0.0	11	40.9	2.3	-24.7	n.d.	n.d.	349	-11.0
ST11	77.12	126.66	0.0	13	29.6	2.9	-28.1	27	13	428	-10.7
ST22	77.67	144.63	0.0	20	11.3	1.1	-28.8	n.d.	95	394	-11.0
ST23	76.43	147.53	0.0	6	7.6	0.9	-28.5	-50	n.d.	394	-11.2
ST24	76.42	149.84	34.4	19	11.9	1.3	-26.8	-62	368	374	-11.1
ST25	76.62	152.03	96.7	23	19.5	1.5	-25.7	-31	465	263	-10.8
ST26	76.14	157.85	96.2	109	30.8	1.2	-24.2	-30	217	316	-10.9
ST27	75.00	161.03	91.5	41	23.3	1.4	-23.0	n.d.	256	299	-11.1
ST28	74.63	161.98	86.3	28	15.5	1.5	-23.8	n.d.	n.d.	214	-11.3
ST29	73.61	169.72	79.3	31	14.7	1.3	-23.2	-50	518	184	-11.3
ST30	75.61	174.01	66.7	43	22.6	2.6	-27.0	n.d.	n.d.	304	-10.5
ST31A	75.85	174.41	75.6	30	10.9	1.1	-21.6	-62	1911	182	-10.6
ST31B	74.26	173.74	63.5	15	4.6	0.6	-23.3	n.d.	783	n.d.	n.d.
ST32	73.56	176.06	51.8	21	11.3	1.3	-24.5	-58	131	n.d.	n.d.
ST33	72.35	-175.14	0.0	20	15.5	2.1	-23.5	n.d.	473	n.d.	n.d.
ST34	73.28	-173.05	28.7	76	13.4	1.6	-21.6	-52	970	n.d.	n.d.
ST35	75.21	-172.05	53.9	24	14.3	1.4	-24.2	n.d.	268	n.d.	n.d.

n.d = not determined

450

451

452

453

454



455

456

457

458

459

Table 2. Surface water (0-20 m) chemical and physical properties during the SWERUS-C3 expedition*

	Salinity	Temperature	DIC	DOC	POC	$\delta^{13}\text{C}$ - DIC	NO_2^- - NO_3^-	PO_4	O_2
		$^\circ\text{C}$	$\mu\text{mol kg}^{-1}$	$\mu\text{mol kg}^{-1}$	$\mu\text{mol kg}^{-1}$	‰	$\mu\text{mol kg}^{-1}$	$\mu\text{mol kg}^{-1}$	$\mu\text{mol kg}^{-1}$
	median	median	median	median	median	median	median	median	median
Outer LS shelf (0-20 m)	32.87	3.84	2139	149.1	7.9	0.75	0.21	0.27	323.0
LS shelf break (0-20 m)	33.56	0.57	2114	91.5	10.1	1.10	0.26	0.15	364.9
Outer ESS shelf (0-20 m)	29.45	-1.33	1969	84.2	10.7	1.14	0.25	0.97	381.5
ESS shelf break (0-20 m)	28.23	-1.32	1979	73.7	4.6	1.47	0.11	0.59	394.1
	mean	mean	mean	mean	mean	mean	mean	mean	mean
Outer LS shelf (0-20 m)	31.17	3.40	2119	179.8	7.9	0.58	0.60	0.29	327.0
LS shelf break (0-20 m)	33.42	0.96	2111	97.5	10.0	1.10	0.61	0.16	358.1
Outer ESS shelf (0-20 m)	28.95	-0.05	1949	95.8	11.9	1.26	0.26	0.95	386.8
ESS shelf break (0-20 m)	28.27	-1.31	1975	72.0	4.6	1.49	0.12	0.60	397.0
	s.d.	s.d.	s.d.	s.d.	s.d.	s.d.	s.d.	s.d.	s.d.
Outer LS shelf (0-20 m)	3.22	2.38	89	66.3	1.7	0.50	0.91	0.11	14.6
LS shelf break (0-20 m)	0.70	2.07	23	21.2	1.7	0.11	0.74	0.06	22.5
Outer ESS shelf (0-20 m)	1.41	2.28	75	30.2	4.6	0.49	0.12	0.19	32.2
ESS shelf break (0-20 m)	0.53	0.04	49	3.2	0.3	0.08	0.03	0.02	8.3

*data from (Humborg et al., submitted; The SWERUS-C3 Scientific Party, 2016)

460

461

462

463

464

465

466

467

468



469

470

471

472

473

Table 3. Qualitative plankton characterization of selected supra-micron POC samples

ID	Region	Diatoms	Dinoflagellates	Other species
ST6	LS	Few <i>Coscinodiscus</i>	None observed	
ST9	LS	None observed	Few <i>Protoperidinium</i>	
ST11	LS	None observed	Abundant <i>Protoperidinium</i>	
ST22	LS-ESS	Abundant <i>Chaetoceros</i> , few <i>Rhizosolenia</i> , <i>Thalassiosira</i>	None observed	
ST25	LS-ESS	High diversity. Abundant <i>Chaetoceros</i> , few <i>Rhizosolenia</i> , <i>Coscinodiscus</i> , <i>Thalassiosira</i> , <i>Asteromphalus</i> , <i>Navicula</i>	None observed	Silicoflagellate
ST31A	ESS	High diversity. Abundant <i>Chaetoceros</i> , few <i>Rhizosolenia</i> , <i>Thalassiosira</i> , <i>Bacterosira</i> , <i>Navicula</i>	None observed	
ST31B	ESS	High diversity. Few <i>Chaetoceros</i> , <i>Thalassiosira</i> , <i>Fragilariopsis</i>	Few <i>Protoperidinium</i>	
ST34	ESS	Abundant <i>Chaetoceros</i> , few <i>Thalassiosira</i> , <i>Navicula</i>	Few <i>Protoperidinium</i>	

474

475

476

477

478

479

480

481

482

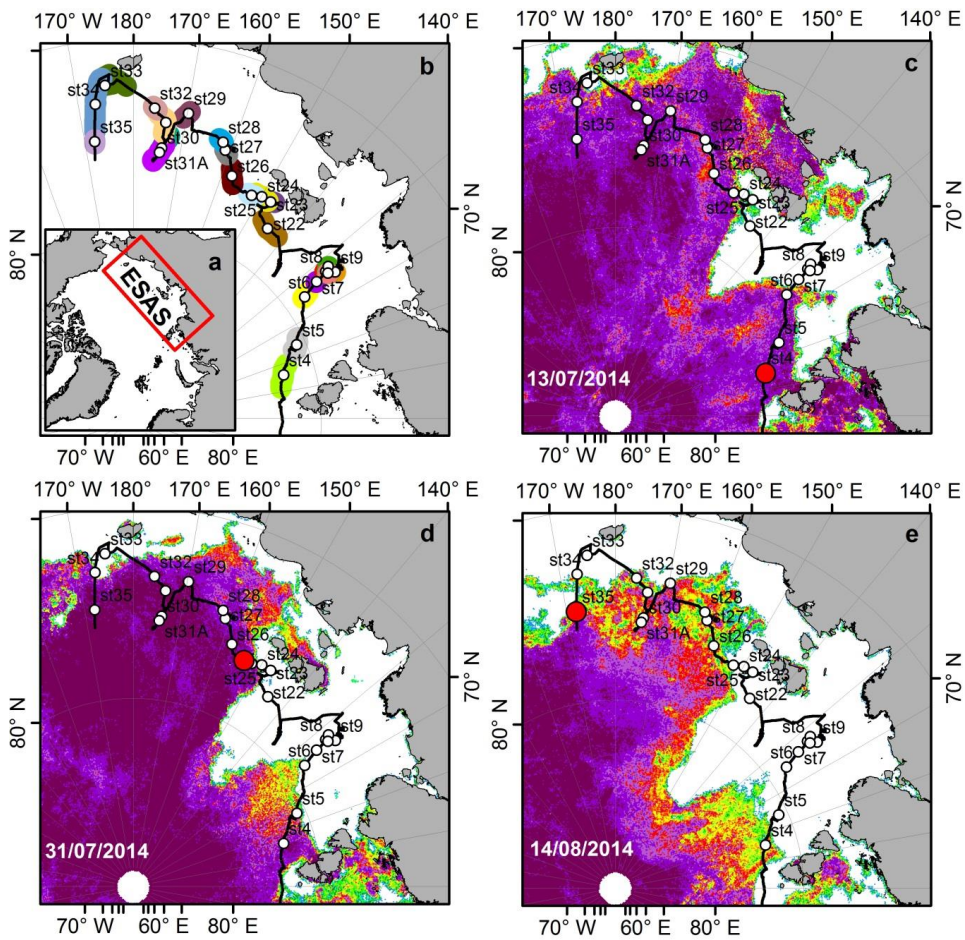
483

484

485



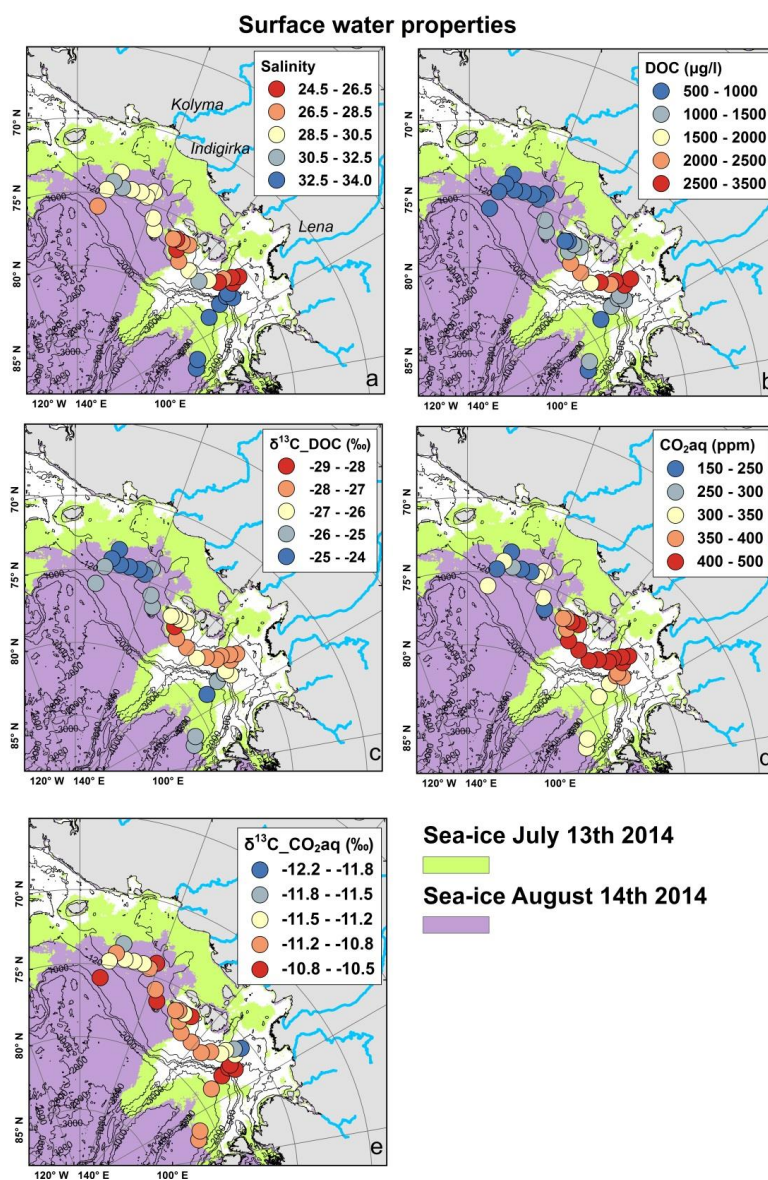
486
 487
 488
 489
 490



491



492 **Fig. 1** (a) The study area in the East Siberian Arctic Shelf. (b) Time-averaged position during
 493 the large-volume filtration (circles) of the supra-POM samples. Shaded coloured areas show
 494 the sampling area covered to harvest each supra-POM sample. Sea-ice extent and
 495 concentration at the beginning (c), in the middle (d) and at the end (e) of the sampling
 496 campaign. The ship position is shown by a filled red circle.

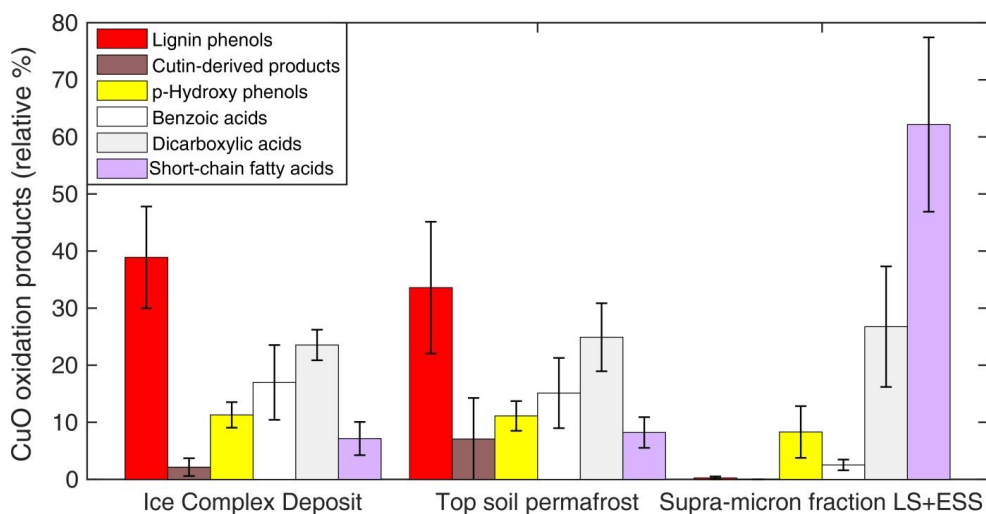


497



498

499 **Fig.2** Surface water properties. (a) Salinity. (b) DOC. (c) $\delta^{13}\text{C}$ -DOC. (d) CO_2aq . (e) $\delta^{13}\text{C}$ -
500 CO_2aq . Shaded areas show the sea-ice extent at the beginning (13/07/2014) and at the end of
501 the sampling campaign (14/08/2014) (Humborg et al., submitted; Salvadó et al., 2016; The
502 SWERUS-C3 Scientific Party, 2016).



503

504

505

506

507 **Fig.3** Alkaline CuO fingerprint of top-soil permafrost samples (Tesi et al., 2014), Pleistocene
508 Ice Complex Deposit (Tesi et al., 2014) and supra-POM fraction (this study). The plot
509 displays the relative proportion of the CuO oxidation products.

510

511

512

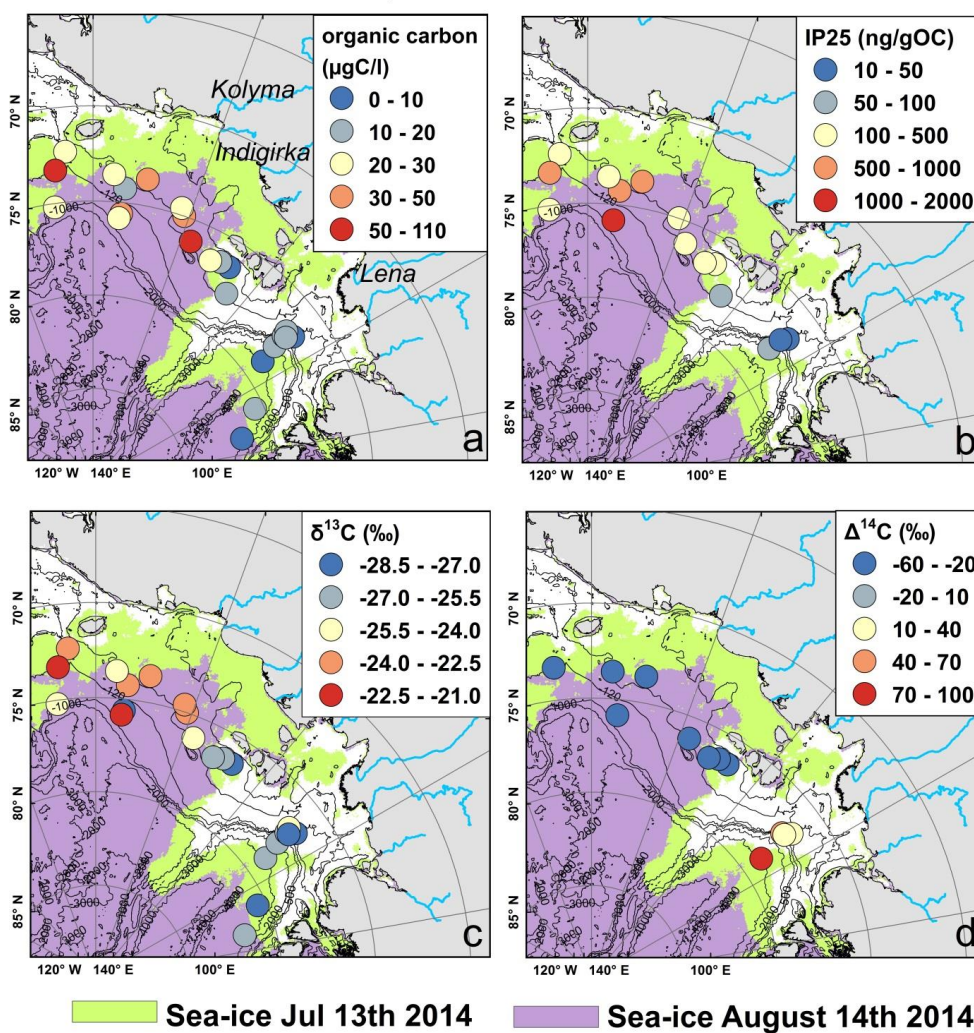
513

514



515
 516
 517
 518
 519

supra-micron POM



520
 521



522 **Fig. 4** Supra-POM composition. (a) Organic carbon concentration. (b) IP25 (mono-
523 unsaturated highly branched isoprenoid. (c) $\delta^{13}\text{C}$. (d) $\Delta^{14}\text{C}$. Shaded areas show the sea-ice
524 extent at the beginning (13/07/2014) and at the end of the sampling campaign (14/08/2014).

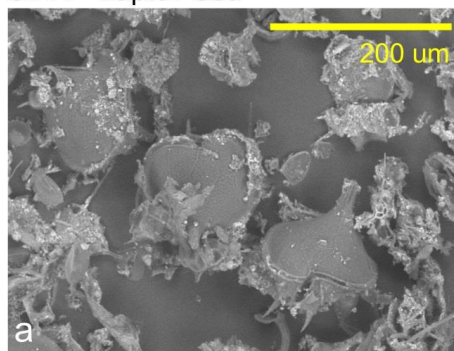
525

526

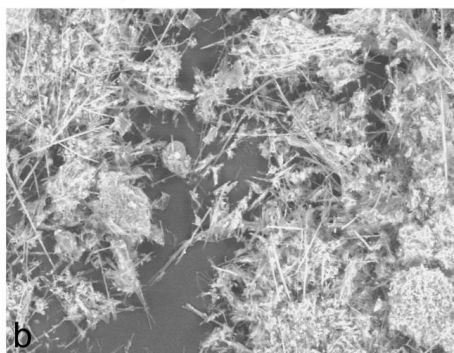
527



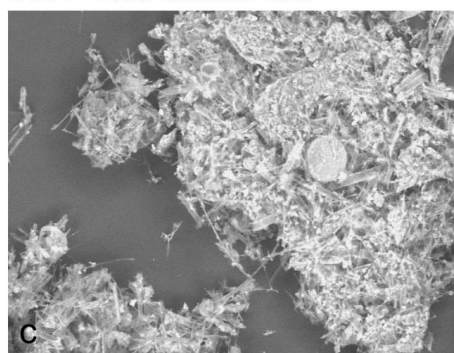
ST11 - Laptev Sea



ST22 - Laptev Sea / East Siberian Sea



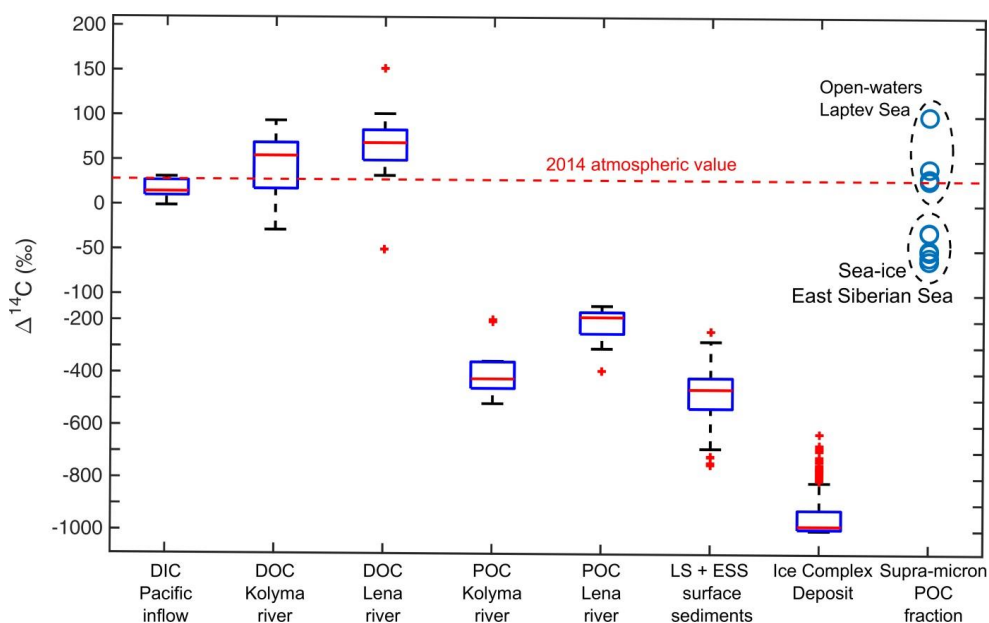
ST34 - East Siberian Sea



528

529

530 **Fig. 5** SEM images. (a) ST-11: Dinoflagellates (*Protoperidinium* spp.) in open-waters of the
531 Laptev Sea. (b) ST22: Diatoms, mostly spines (setae) of *Chaetoceros* spp. in the transition
532 between Laptev Sea and East Siberian Sea. (c) ST-34: Diatoms from sea-ice dominated
533 waters in the East Siberian Sea



534

535

536

537 **Fig. 6** Radiocarbon signature of inorganic and organic carbon pools. Whisker plots of
 538 radiocarbon values for different inorganic and organic carbon sources from the literature,
 539 compared to the outer Laptev Sea and outer East Siberian Sea (blue circles, this study). Solid
 540 lines show the median, the box limits display the 25th and 75th percentiles while the crosses
 541 show the outliers. Source: DIC (Griffith et al., 2012), DOC-Kolyma (2009-2014), DOC-Lena
 542 (2009-2014), POC-Kolyma (2009-2011), POC-Lena (2009-2011)
 543 (www.arcticgreatrivers.org), Laptev Sea and Eastern Siberia Sea surface sediments (Salvadó
 544 et al., 2016; Vonk et al., 2012) and Ice Complex Deposit (Vonk et al., 2012).

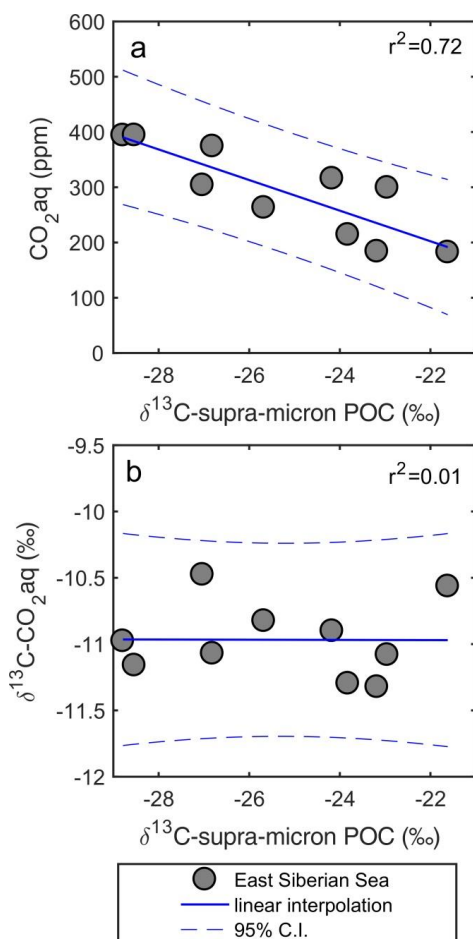
545

546

547

548

549



550

551

552

553 **Fig. 7** Correlations (a) CO_2aq vs $\delta^{13}\text{C}$ (supra-micron POM fraction) and (b) $\delta^{13}\text{C}\text{-CO}_2\text{aq}$ vs

554 $\delta^{13}\text{C}$ in the East Siberian Sea (filled circles). The solid line shows the linear interpolation

555 while the dashed line shows the 95% confidence intervals.

556

557

558

559

560 **References**

- 561 Aagaard, K. and Carmack, E. C.: The role of sea ice and other fresh water in the Arctic circulation,
562 *Journal of Geophysical Research: Oceans*, 94, 14485-14498, 1989.
- 563 Alling, V., Sanchez-Garcia, L., Porcelli, D., Pugach, S., Vonk, J. E., van Dongen, B., Mörth, C.-M.,
564 Anderson, L. G., Sokolov, A., Andersson, P., Humborg, C., Semiletov, I., and Gustafsson, Ö.:
565 Nonconservative behavior of dissolved organic carbon across the Laptev and East Siberian seas,
566 *Global Biogeochemical Cycles*, 24, n/a-n/a, 2010.
- 567 Amon, R., Rinehart, A., Duan, S., Louchouart, P., Prokushkin, A., Guggenberger, G., Bauch, D.,
568 Stedmon, C., Raymond, P., and Holmes, R.: Dissolved organic matter sources in large Arctic rivers,
569 *Geochimica et Cosmochimica Acta*, 94, 217-237, 2012.
- 570 Anderson, L. G., Jutterström, S., Hjalmarsson, S., Wåhlström, I., and Semiletov, I.: Out-gassing of CO₂
571 from Siberian Shelf seas by terrestrial organic matter decomposition, *Geophysical Research Letters*,
572 36, 2009.
- 573 Ardyna, M., Babin, M., Gosselin, M., Devred, E., Rainville, L., and Tremblay, J. É.: Recent Arctic Ocean
574 sea ice loss triggers novel fall phytoplankton blooms, *Geophysical Research Letters*, 41, 6207-6212,
575 2014.
- 576 Arrigo, K. R., van Dijken, G., and Pabi, S.: Impact of a shrinking Arctic ice cover on marine primary
577 production, *Geophysical Research Letters*, 35, n/a-n/a, 2008.
- 578 Belt, S. T., Brown, T. A., Rodriguez, A. N., Sanz, P. C., Tonkin, A., and Ingle, R.: A reproducible method
579 for the extraction, identification and quantification of the Arctic sea ice proxy IP25 from marine
580 sediments, *Analytical Methods*, 4, 705-713, 2012.
- 581 Belt, S. T., Massé, G., Rowland, S. J., Poulin, M., Michel, C., and LeBlanc, B.: A novel chemical fossil of
582 palaeo sea ice: IP25, *Organic Geochemistry*, 38, 16-27, 2007.
- 583 Björk, G., Jutterström, S., Pipko, I., Shakhova, N., Semiletov, I., and Wåhlström, I.: East Siberian Sea,
584 an Arctic region of very high biogeochemical activity, *Biogeosciences*, 8, 1745, 2011.
- 585 Bröder, L., Tesi, T., Andersson, A., Eglinton, T. I., Semiletov, I. P., Dudarev, O. V., Roos, P., and
586 Gustafsson, Ö.: Historical records of organic matter supply and degradation status in the East
587 Siberian Sea, *Organic Geochemistry*, 91, 16-30, 2016a.
- 588 Bröder, L., Tesi, T., Salvadó, J. A., Semiletov, I. P., Dudarev, O. V., and Gustafsson, Ö.: Fate of
589 terrigenous organic matter across the Laptev Sea from the mouth of the Lena River to the deep sea
590 of the Arctic interior, *Biogeosciences*, 13, 5003-5019, 2016b.
- 591 Brown, T. A., Belt, S. T., Tatarek, A., and Mundy, C. J.: Source identification of the Arctic sea ice proxy
592 IP25, *Nature Communications*, 5, 4197, 2014.
- 593 Carlsson, P., Graneli, E., Tester, P., and Boni, L.: Influences of riverine humic substances on bacteria,
594 protozoa, phytoplankton, and copepods in a coastal plankton community, *Marine Ecology Progress
595 Series*, 127, 213-221, 1995.
- 596 Comiso, J. C., Parkinson, C. L., Gersten, R., and Stock, L.: Accelerated decline in the Arctic sea ice
597 cover, *Geophysical research letters*, 35, 2008.
- 598 Dittmar, T. and Kattner, G.: The biogeochemistry of the river and shelf ecosystem of the Arctic
599 Ocean: a review, *Marine chemistry*, 83, 103-120, 2003.
- 600 Dunton, K. H., Weingartner, T., and Carmack, E. C.: The nearshore western Beaufort Sea ecosystem:
601 Circulation and importance of terrestrial carbon in arctic coastal food webs, *Progress in
602 Oceanography*, 71, 362-378, 2006.



- 603 Feng, X., Gustafsson, Ö., Holmes, R. M., Vonk, J. E., van Dongen, B. E., Semiletov, I. P., Dudarev, O. V.,
604 Yunker, M. B., Macdonald, R. W., Wacker, L., Montluçon, D. B., and Eglinton, T. I.: Multimolecular
605 tracers of terrestrial carbon transfer across the pan-Arctic: 14C characteristics of sedimentary carbon
606 components and their environmental controls, *Global Biogeochemical Cycles*, 29, 1855-1873, 2015.
- 607 Fichot, C. G., Kaiser, K., Hooker, S. B., Amon, R. M., Babin, M., Bélanger, S., Walker, S. A., and Benner,
608 R.: Pan-Arctic distributions of continental runoff in the Arctic Ocean, *Scientific reports*, 3, 1053, 2013.
- 609 Frey, K. E. and Smith, L. C.: Amplified carbon release from vast West Siberian peatlands by 2100,
610 *Geophysical Research Letters*, 32, 2005.
- 611 Fujiwara, A., Hirawake, T., Suzuki, K., Imai, I., and Saitoh, S.-I.: Timing of sea ice retreat can alter
612 phytoplankton community structure in the western Arctic Ocean, *Biogeosciences*, 11, 1705-1716,
613 2014.
- 614 Gervais, F. and Riebesell, U.: Effect of phosphorus limitation on elemental composition and stable
615 carbon isotope fractionation in a marine diatom growing under different CO₂ concentrations,
616 *Limnology and Oceanography*, 46, 497-504, 2001.
- 617 Goñi, M. A. and Hedges, J. I.: Potential applications of cutin-derived CuO reaction products for
618 discriminating vascular plant sources in natural environments, *Geochimica et Cosmochimica Acta*, 54,
619 3073-3081, 1990.
- 620 Goñi, M. A. and Hedges, J. I.: Sources and reactivities of marine-derived organic matter in coastal
621 sediments as determined by alkaline CuO oxidation, *Geochimica et Cosmochimica Acta*, 59, 2965-
622 2981, 1995.
- 623 Griffith, D. R., McNichol, A. P., Xu, L., McLaughlin, F. A., Macdonald, R. W., Brown, K. A., and Eglinton,
624 T. I.: Carbon dynamics in the western Arctic Ocean: insights from full-depth carbon isotope profiles of
625 DIC, DOC, and POC, 2012. 2012.
- 626 Gustafsson, Ö., Andersson, P., Axelman, J., Bucheli, T., Kömp, P., McLachlan, M., Sobek, A., and
627 Thörngren, J.-O.: Observations of the PCB distribution within and in-between ice, snow, ice-rafted
628 debris, ice-interstitial water, and seawater in the Barents Sea marginal ice zone and the North Pole
629 area, *Science of the total environment*, 342, 261-279, 2005.
- 630 Gustafsson, Ö. and Andersson, P. S.: 234Th-derived surface export fluxes of POC from the Northern
631 Barents Sea and the Eurasian sector of the Central Arctic Ocean, *Deep Sea Research Part I:
632 Oceanographic Research Papers*, 68, 1-11, 2012.
- 633 Hoins, M., Van de Waal, D. B., Eberlein, T., Reichart, G.-J., Rost, B., and Sluijs, A.: Stable carbon
634 isotope fractionation of organic cyst-forming dinoflagellates: Evaluating the potential for a CO₂
635 proxy, *Geochimica et Cosmochimica Acta*, 160, 267-276, 2015.
- 636 Humborg, C., Marc C. Geibel, Anderson, L. G., Göran Björk, Mörth, C.-M., Sundbom, M., Thornton, B.
637 F., Crill, P. M., Deutsch, B., Gustafsson, E., Gustafsson, B., Ek, J., and Semiletov, I.: Sea-air exchange
638 patterns along the central and outer East Siberian Arctic Shelf as inferred from continuous CO₂,
639 stable isotope and bulk chemistry measurements *Global Biogeochemical Cycles*, submitted.
640 submitted.
- 641 Iken, K., Bluhm, B., and Gradinger, R.: Food web structure in the high Arctic Canada Basin: evidence
642 from $\delta^{13}\text{C}$ and $\delta^{15}\text{N}$ analysis, *Polar Biology*, 28, 238-249, 2005.
- 643 Janout, M. A., Hölemann, J., Waite, A. M., Krumpfen, T., Appen, W. J., and Martynov, F.: Sea-ice
644 retreat controls timing of summer plankton blooms in the Eastern Arctic Ocean, *Geophysical
645 Research Letters*, 2016. 2016.



- 646 Karlsson, E., Gelting, J., Tesi, T., Dongen, B., Andersson, A., Semiletov, I., Charkin, A., Dudarev, O., and
647 Gustafsson, Ö.: Different sources and degradation state of dissolved, particulate and sedimentary
648 organic matter along the Eurasian Arctic coastal margin, *Global Biogeochemical Cycles*, 2016. 2016.
- 649 Kohlbach, D., Graeve, M., A Lange, B., David, C., Peeken, I., and Flores, H.: The importance of ice
650 algae-produced carbon in the central Arctic Ocean ecosystem: Food web relationships revealed by
651 lipid and stable isotope analyses, *Limnology and Oceanography*, 2016. 2016.
- 652 Kwok, R. and Rothrock, D.: Decline in Arctic sea ice thickness from submarine and ICESat records:
653 1958–2008, *Geophysical Research Letters*, 36, 2009.
- 654 Lalande, C., Bélanger, S., and Fortier, L.: Impact of a decreasing sea ice cover on the vertical export of
655 particulate organic carbon in the northern Laptev Sea, Siberian Arctic Ocean, *Geophysical Research
656 Letters*, 36, n/a-n/a, 2009.
- 657 Lalande, C., Nöthig, E. M., Somavilla, R., Bauerfeind, E., Shevchenko, V., and Okolodkov, Y.: Variability
658 in under-ice export fluxes of biogenic matter in the Arctic Ocean, *Global Biogeochemical Cycles*, 28,
659 571-583, 2014.
- 660 Laws, E. A., Bidigare, R. R., and Popp, B. N.: Effect of growth rate and CO₂ concentration on carbon
661 isotopic fractionation by the marine diatom *Phaeodactylum tricornutum*, *Limnology and
662 Oceanography*, 42, 1552-1560, 1997a.
- 663 Laws, E. A., Bidigare, R. R., and Popp, B. N.: Effect of growth rate and CO₂ concentration on carbon
664 isotopic fractionation by the marine diatom *Phaeodactylum tricornutum*, 1997b. 1997b.
- 665 Laws, E. A., Popp, B. N., Bidigare, R. R., Kennicutt, M. C., and Macko, S. A.: Dependence of
666 phytoplankton carbon isotopic composition on growth rate and [CO₂] aq: Theoretical considerations
667 and experimental results, *Geochimica et cosmochimica acta*, 59, 1131-1138, 1995.
- 668 McClelland, J. W., Holmes, R. M., Peterson, B. J., Raymond, P. A., Striegl, R., Zhulidov, A. V., Zimov, S.,
669 Zimov, N., Tank, S. E., and Spencer, R. G.: Particulate organic carbon and nitrogen export from major
670 Arctic rivers, *Global Biogeochemical Cycles*, 30, 629-643, 2016.
- 671 Nieuwenhuize, J., Maas, Y. E., and Middelburg, J. J.: Rapid analysis of organic carbon and nitrogen in
672 particulate materials, *Marine Chemistry*, 45, 217-224, 1994.
- 673 Pagani, M., Arthur, M. A., and Freeman, K. H.: Miocene evolution of atmospheric carbon dioxide,
674 *Paleoceanography*, 14, 273-292, 1999.
- 675 Pipko, I. I., Pugach, S. P., and Semiletov, I. P.: The autumn distribution of the CO₂ partial pressure in
676 bottom waters of the East Siberian Sea, *Doklady Earth Sciences*, 425, 345-349, 2009.
- 677 Popp, B. N., Laws, E. A., Bidigare, R. R., Dore, J. E., Hanson, K. L., and Wakeham, S. G.: Effect of
678 phytoplankton cell geometry on carbon isotopic fractionation, *Geochimica et cosmochimica acta*, 62,
679 69-77, 1998.
- 680 Popp, B. N., Trull, T., Kenig, F., Wakeham, S. G., Rust, T. M., Tilbrook, B., Griffiths, B., Wright, S. W.,
681 Marchant, H. J., and Bidigare, R. R.: Controls on the carbon isotopic composition of Southern Ocean
682 phytoplankton, *Global Biogeochemical Cycles*, 13, 827-843, 1999.
- 683 Purina, I., Balode, M., Béchemin, C., Pöder, T., Vérité, C., and Maestrini, S.: Influence of dissolved
684 organic matter from terrestrial origin on the changes of dinoflagellate species composition in the Gulf
685 of Riga, Baltic Sea, *Hydrobiologia*, 514, 127-137, 2004.
- 686 Rau, G., Riebesell, U., and Wolf-Gladrow, D.: A model of photosynthetic ¹³C fractionation by marine
687 phytoplankton based on diffusive molecular CO₂ uptake, *Marine Ecology Progress Series*, 133, 275-
688 285, 1996.



- 689 Rau, G. H.: Variations in sedimentary organic $\delta^{13}\text{C}$ as a proxy for past changes in ocean and
690 atmospheric CO_2 concentrations. In: Carbon Cycling in the Glacial Ocean: Constraints on the Ocean's
691 Role in Global Change, Springer, 1994.
- 692 Salvadó, J. A., Tesi, T., Sundbom, M., Karlsson, E., Kruså, M., Semiletov, I. P., Panova, E., and
693 Gustafsson, Ö.: Contrasting composition of terrigenous organic matter in the dissolved, particulate
694 and sedimentary organic carbon pools on the outer East Siberian Arctic Shelf, *Biogeosciences*, 13,
695 6121-6138, 2016.
- 696 Sánchez-García, L., Alling, V., Pugach, S., Vonk, J., van Dongen, B., Humborg, C., Dudarev, O.,
697 Semiletov, I., and Gustafsson, Ö.: Inventories and behavior of particulate organic carbon in the
698 Laptev and East Siberian seas, *Global Biogeochemical Cycles*, 25, 2011.
- 699 Semiletov, I., Dudarev, O., Luchin, V., Charkin, A., Shin, K. H., and Tanaka, N.: The East Siberian Sea as
700 a transition zone between Pacific-derived waters and Arctic shelf waters, *Geophysical Research*
701 *Letters*, 32, 2005.
- 702 Semiletov, I., Pipko, I., Gustafsson, O., Anderson, L. G., Sergienko, V., Pugach, S., Dudarev, O.,
703 Charkin, A., Gukov, A., Broder, L., Andersson, A., Spivak, E., and Shakhova, N.: Acidification of East
704 Siberian Arctic Shelf waters through addition of freshwater and terrestrial carbon, *Nature Geosci*, 9,
705 361-365, 2016.
- 706 Semiletov, I. P., Shakhova, N. E., Pipko, I. I., Pugach, S. P., Charkin, A. N., Dudarev, O. V., Kosmach, D.
707 A., and Nishino, S.: Space-time dynamics of carbon and environmental parameters related to carbon
708 dioxide emissions in the Buor-Khaya Bay and adjacent part of the Laptev Sea, *Biogeosciences*, 10,
709 5977, 2013.
- 710 Sobek, A. and Gustafsson, Ö.: Latitudinal fractionation of polychlorinated biphenyls in surface
711 seawater along a 62 N– 89 N transect from the southern Norwegian Sea to the North Pole area,
712 *Environmental science & technology*, 38, 2746-2751, 2004.
- 713 Spreen, G., Kaleschke, L., and Heygster, G.: Sea ice remote sensing using AMSR-E 89-GHz channels,
714 *Journal of Geophysical Research: Oceans*, 113, 2008.
- 715 Tesi, T., Muschitiello, F., Smittenberg, R. H., Jakobsson, M., Vonk, J. E., Hill, P., Andersson, A.,
716 Kirchner, N., Noormets, R., Dudarev, O., Semiletov, I., and Gustafsson, Ö.: Massive remobilization of
717 permafrost carbon during post-glacial warming, *Nature Communications*, 7, 13653, 2016.
- 718 Tesi, T., Puig, P., Palanques, A., and Goñi, M.: Lateral advection of organic matter in cascading-
719 dominated submarine canyons, *Progress in Oceanography*, 84, 185-203, 2010.
- 720 Tesi, T., Semiletov, I., Hugelius, G., Dudarev, O., Kuhry, P., and Gustafsson, Ö.: Composition and fate
721 of terrigenous organic matter along the Arctic land–ocean continuum in East Siberia: Insights from
722 biomarkers and carbon isotopes, *Geochimica et Cosmochimica Acta*, 133, 235-256, 2014.
- 723 The SWERUS-C3 Scientific Party: The SWERUS-C3 Scientific Party (2016) The Swedish-Russian-US
724 Investigation of Climate-Cryosphere-Carbon Interactions in the East Siberian Arctic Ocean. The
725 SWERUS-C3 2014 Expedition Cruise Report Leg 1 (of 2). , Stockholm University, Stockholm, Sweden,
726 2016.978-91-87355-20-2
- 727 Vonk, J., Sánchez-García, L., Van Dongen, B., Alling, V., Kosmach, D., Charkin, A., Semiletov, I. P.,
728 Dudarev, O. V., Shakhova, N., and Roos, P.: Activation of old carbon by erosion of coastal and subsea
729 permafrost in Arctic Siberia, *Nature*, 489, 137-140, 2012.
- 730 Vonk, J. E., Semiletov, I. P., Dudarev, O. V., Eglinton, T. I., Andersson, A., Shakhova, N., Charkin, A.,
731 Heim, B., and Gustafsson, Ö.: Preferential burial of permafrost-derived organic carbon in Siberian-
732 Arctic shelf waters, *Journal of Geophysical Research: Oceans*, 119, 8410-8421, 2014.



733 Wegner, C., Hölemann, J. A., Dmitrenko, I., Kirillov, S., Tuschling, K., Abramova, E., and Kassens, H.:
734 Suspended particulate matter on the Laptev Sea shelf (Siberian Arctic) during ice-free conditions,
735 Estuarine, Coastal and Shelf Science, 57, 55-64, 2003.

736 Wikner, J. and Andersson, A.: Increased freshwater discharge shifts the trophic balance in the coastal
737 zone of the northern Baltic Sea, Global Change Biology, 18, 2509-2519, 2012.

738 Wolf-Gladrow, D. A., Riebesell, U., Burkhardt, S., and Bijma, J.: Direct effects of CO₂ concentration on
739 growth and isotopic composition of marine plankton, Tellus B, 51, 461-476, 1999.

740

741